AIP Journal of Applied Physics

Electron and phonon transport in Co-doped FeV0.6Nb0.4Sb half-Heusler thermoelectric materials

Chenguang Fu, Yintu Liu, Hanhui Xie, Xiaohua Liu, Xinbing Zhao, G. Jeffrey Snyder, Jian Xie, and Tiejun Zhu

Citation: Journal of Applied Physics **114**, 134905 (2013); doi: 10.1063/1.4823859
View online: http://dx.doi.org/10.1063/1.4823859
View Table of Contents: http://scitation.aip.org/content/aip/journal/jap/114/13?ver=pdfcov
Published by the AIP Publishing

Electron and phonon transport in Co-doped $FeV_{0.6}Nb_{0.4}Sb$ half-Heusler thermoelectric materials

Chenguang Fu,[1] Yintu Liu,[1] Hanhui Xie,[1] Xiaohua Liu,[1] Xinbing Zhao,[1,2] G. Jeffrey Snyder,[3] Jian Xie,[1,2] and Tiejun Zhu[1,2,a)]

[1]*State Key Laboratory of Silicon Materials and Department of Materials Science and Engineering, Zhejiang University, Hangzhou 310027, China*

[2]*Key Laboratory of Advanced Materials and Applications for Batteries of Zhejiang Province, Zhejiang University, Hangzhou 310027, China*

[3]*Materials Science, California Institute of Technology, Pasadena, California 91125, USA*

(Received 4 July 2013; accepted 16 September 2013; published online 4 October 2013)

The electron and phonon transport characteristics of n-type $Fe_{1-x}Co_xV_{0.6}Nb_{0.4}Sb$ half-Heusler thermoelectric compounds is analyzed. The acoustic phonon scattering is dominant in the carrier transport. The deformation potential of $E_{def} = 14.1$ eV and the density of state effective mass $m^* \approx 2.0\, m_e$ are derived under a single parabolic band assumption. The band gap is calculated to be ~0.3 eV. Electron and phonon mean free paths are estimated based on the low and high temperature measurements. The electron mean free path is higher than the phonon one above room temperature, which is consistent with the experimental result that the electron mobility decreases more than the lattice thermal conductivity by grain refinement to enhance boundary scattering. A maximum *ZT* value of ~0.33 is obtained at 650 K for $x = 0.015$, an increase by ~60% compared with FeVSb. The optimal doping level is found to be $\sim 3.0 \times 10^{20}\ cm^{-3}$ at 600 K. © *2013 AIP Publishing LLC*. [http://dx.doi.org/10.1063/1.4823859]

I. INTRODUCTION

Half-Heusler phases are an attractive class of intermetallic compounds with the cubic MgAgAs crystal structure (space group $F\bar{4}3m$).[1] These compounds cover various promising candidates as half-metallic magnetic semiconductors,[2–4] shape memory alloys,[5] piezoelectric materials,[6] and topological insulators.[7,8] In recent years, the half-Heusler compounds with valence electron count VEC = 18 have been identified as potential high temperature thermoelectric (TE) materials for power generation.[9–13] The performance of a TE material is represented by the dimensionless figure of merit $ZT = S^2\sigma T/(\kappa_e + \kappa_L)$, where S, σ, T, κ_e, and κ_L are, respectively, the Seebeck coefficient, the electrical conductivity, the absolute temperature, and the electrical and lattice components of total thermal conductivity κ.[14] It is difficult to optimize these variables independently to increase *ZT* because the quantities S, σ, and κ_e are interrelated via carrier concentration. The compromise between a large Seebeck coefficient and a high electrical conductivity for promising thermoelectric materials with high *ZT* requires an optimal carrier concentration between 10^{19} and 10^{21} carriers per cm^3, which is usually found in heavily doped semiconductors.[15] The κ_L is independent of the electrical properties, which should be minimized as much as possible. Therefore, there are usually two approaches to optimize the performance of a TE material: One is to reduce the lattice thermal conductivity by alloying or nanostructuring to induce point defects[16,17] or interfaces,[18–20] and the other is to optimize the power factor $PF\ \alpha^2\sigma$ by band engineering, such as modification of electron states via resonant levels,[21,22] convergence of energy bands,[23–25] or weakening the scattering of carriers.[26,27]

MNiSn (M = Ti, Zr, Hf)[9,16,17,28–30] and MCoSb[31,32] compounds are most widely investigated half-Heusler TE materials due to their high Seebeck coefficients and moderate electrical conductivities. And the state-of-the-art *ZT* values of close to unity have been obtained at high temperatures.[33,34] Another half-Heusler compound, FeVSb, usually exhibits the maximum *ZT* value in medium temperature range (550–750 K). Despite of its high power factor, $\sim 4 \times 10^{-3}\ W\ m^{-1}\ K^{-2}$ at 300 K, the relatively high thermal conductivity ($\kappa \approx 10\ W\ m^{-1}\ K^{-1}$) makes this system less promising for TE application at present.[35] In our previous study, the enhanced point defect scattering for phonons has been introduced by the isoelectronic substitution of Nb on the V sites. A significantly reduced thermal conductivity of $5.5\ W\ m^{-1}\ K^{-1}$ for the $FeV_{0.6}Nb_{0.4}Sb$ was obtained at 300 K. However, the simultaneous decrease in electrical conductivity leads to deteriorated power factor and *ZT*.[36] The optimal TE figure of merit $ZT \propto \mu m^{*3/2}/\kappa_L$ is related to the carriers mobility μ, the density-of-states effective mass m^*, and the lattice thermal conductivity κ_L. The knowledge of electron and phonon transport mechanisms would provide important guidelines for the improvement of the TE performance of this system.

In this work, we study the electron and phonon transport characteristics of n-type $Fe_{1-x}Co_xV_{0.6}Nb_{0.4}Sb$ ($x = 0 \sim 0.02$) compounds. The Co doping on the Fe site can increase the electron concentration and improve conductivity. Since previous energy band calculation shows that the FeVSb and FeNbSb have single conduction bands,[12,37] the single parabolic band (SPB) model, which is combined with the solution to the Boltzmann transport equation within the relaxation

a)Author to whom correspondence should be addressed. Email: zhutj@zju.edu.cn. Tel: ++86-571-87952181. Fax: +86-571-87951203.

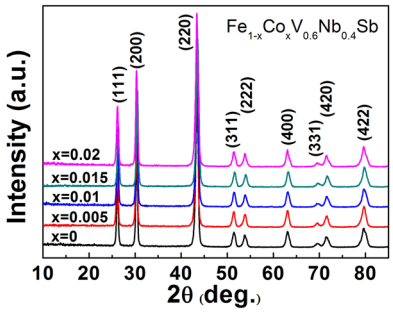

FIG. 1. XRD pattern of $Fe_{1-x}Co_xV_{0.6}Nb_{0.4}Sb$ ($x = 0$, 0.005, 0.01, 0.015, 0.02) samples.

time approximation,[38] is employed to analyze the electrical transport properties of the compounds. Moreover, the electron mean free path (EMFP) of $Fe_{1-x}Co_xV_{0.6}Nb_{0.4}Sb$ and phonon mean free path (PMFP) are evaluated. Both the calculated and experimental results indicate that the μ/κ_L ratio is not improved by enhancing boundary scattering in this system.

II. EXPERIMENTAL PROCEDURES

$Fe_{1-x}Co_xV_{0.6}Nb_{0.4}Sb$ ($x = 0$, 0.005, 0.01, 0.015, 0.02) ingots were prepared by levitation melting. More details can be found elsewhere.[33,35] The ingots were pulverized and sifted through a 200 mesh sieve. Two samples with $x = 0.01$ and $x = 0.015$ were further pulverized by ball milling (BM) for 10 h to obtain fine-grained powders for comparison. The powders were compacted by spark plasma sintering (SPS-1050, Sumitomo Coal Mining Co.) at 1073 K for 10 min under 65 MPa. The obtained sample pellets were annealed at 1023 K for 2 days. The relative density of all samples was found to be ~95%.

Phase structure of the samples was investigated by X-ray diffraction (XRD) on a RigakuD/MAX-2550PC diffractometer. The XRD analysis, as shown in Fig. 1, indicates that no impurity phases exist in the samples. No obvious change in lattice parameter was observed since the Co has similar radius with Fe. Compositional homogeneity of all samples was examined by electron probe microanalysis (EPMA, JEOL JXA-8100). The sample pellets of 12.7 mm in diameter were used to measure the thermal conductivity and then cut into the rectangular bars for the electrical property measurements. The Seebeck coefficient and electrical conductivity from 300–800 K were measured on a commercial Linseis LSR-3 system using a differential voltage/temperature technique and DC four-probe method, respectively. The thermal conductivity κ was calculated from $\kappa = D\rho C_p$, where ρ is the sample density estimated by the Archimedes method. The thermal diffusivity D and specific heat C_p were measured by a laser flash method on Netzsch LFA457 instrument with a Pyroceram standard. The low temperature Hall coefficients R_H and thermal conductivity of the samples were measured using a physical property measurement system (PPMS-9T, Quantum Design Inc., USA). The carrier concentration n_H was calculated by $n_H = 1/eR_H$, where e is the unit charge. The carriers mobility μ_H was calculated by $\mu_H = \sigma R_H$.

III. ELECTRICAL TRANSPORT

Figure 2 shows the electrical properties of $Fe_{1-x}Co_xV_{0.6}Nb_{0.4}Sb$ ($x = 0 \sim 0.02$) compounds. The parent

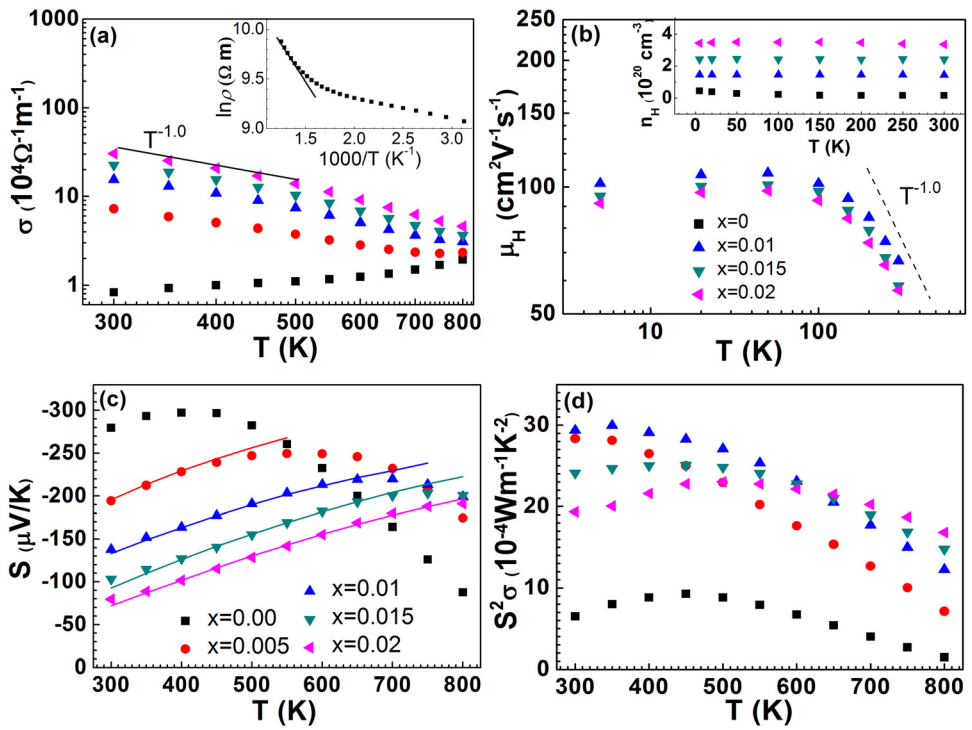

FIG. 2. Temperature dependences of electrical conductivity (a), Hall mobility (b), Seebeck coefficient (c), and power factor (d) of $Fe_{1-x}Co_xV_{0.6}Nb_{0.4}Sb$ samples. The inset in (b) shows the temperature dependence of Hall carrier concentration. Inset of Fig. 2(a) shows $\ln\rho \sim 1/T$ relationship for $FeV_{0.6}Nb_{0.4}Sb$. In Fig. 2(c), the solid curves for samples $x = 0.005-0.02$ were calculated using SPB model. A good agreement is displayed between the calculated curves and experimental data before the intrinsic excitation.

sample $FeV_{0.6}Nb_{0.4}Sb$, without Co doping, possesses a high Seebeck coefficient of $-280\,\mu V/K$ and a small electrical conductivity of $0.8\times10^4\,\Omega^{-1}\,m^{-1}$ at room temperature. The temperature dependence of resistivity of $FeV_{0.6}Nb_{0.4}Sb$ at high temperatures follows a simple exponent law $\rho=\rho_0\exp(E_g/2k_BT)$, where E_g is the band gap and k_B is the Boltzmann constant (the inset of Fig. 2(a)). The determined value for E_g is ~0.26 eV. Co acts as an effective donor and improves the electrical conductivity, as shown in Fig. 2(a). The electrical conductivity for all the Co doped samples decreases with increasing temperature, revealing a metal-like behavior. The σ of the Co doped samples follows a power law of $\sigma\sim T^{-1.0}$ below ~500 K. The Hall carrier concentration of the samples below 300 K, shown in Fig. 2(b), keeps nearly constant. The Hall mobility follows a relationship $\mu_H\sim T^{-1.0}$ near room temperature, consistent with the temperature dependence of electrical conductivity, indicating that the acoustic phonon scattering of carriers may be dominant in degenerate $Fe_{1-x}Co_xV_{0.6}Nb_{0.4}Sb$ ($x>0.005$) compounds.[39]

The absolute Seebeck coefficient of all the samples decreases with increasing carrier concentration, in Fig. 2(c). The Seebeck coefficient of the Co doped samples increases linearly with increasing temperature before the intrinsic excitation. The temperature T_{max}, at which the maximum Seebeck coefficient occurs, increases with increasing Co content, implying that the intrinsic excitation occurs at higher temperatures. The band gap of all the samples can be estimated by the formula $S_{max}=E_g/2eT_{max}$,[40] where T_{max} is the temperature that the maximum Seebeck coefficient S_{max} occurs. The calculated E_g of ~0.3 eV for all the samples is close to that for $FeV_{0.6}Nb_{0.4}Sb$ (~0.26 eV), and is also similar to the band gap of ZrNiSn (~0.3 eV).[28] Fig. 2(d) shows the power factor of all the Co doped samples is enhanced, especially near room temperature, increasing from $6.5\times10^{-4}\,W\,m^{-1}\,K^{-2}$ for $x=0$ to $29.3\times10^{-4}\,W\,m^{-1}\,K^{-2}$ for sample $x=0.01$.

Within the framework of a single parabolic band assumption, the Seebeck coefficient S and Hall carrier concentration n_H are given by

$$S=-\frac{k_B}{e}\left[\frac{(5/2+\lambda)F_{\lambda+3/2}(\eta)}{(3/2+\lambda)F_{\lambda+1/2}(\eta)}-\eta\right], \tag{1}$$

$$n_H=\frac{4\pi(2m*k_BT)^{3/2}}{h^3}\frac{F_{1/2}(\eta)}{r_H}, \tag{2}$$

$$r_H=\frac{3}{2}F_{1/2}(\eta)\frac{(3/2+2\lambda)F_{2\lambda+1/2}(\eta)}{(3/2+\lambda)^2F^2_{\lambda+1/2}(\eta)}, \tag{3}$$

$$F_i(\eta)=\int_0^\infty\frac{\xi^i d\xi}{1+\exp(\xi-\eta)}, \tag{4}$$

where $\eta=E_F/k_BT$ is the reduced Fermi level, ζ the reduced carrier energy, $F_i(\eta)$ the Fermi-Dirac integral, r_H the Hall factor, m^* the density of states effective mass, h the Planck constant, and the scattering factor λ relates to the energy dependence of the carrier relaxation time τ via $\tau=\tau_0\cdot\varepsilon^\lambda$.[41,42] The acoustic phonon scattering gives $\lambda=-1/2$. Based on the experimental Seebeck coefficients and carrier concentrations, an effective mass $m^*\approx2.0\,m_e$ was derived for all $Fe_{1-x}Co_xV_{0.6}Nb_{0.4}Sb$ ($x>0$) samples using Eqs. (1)–(4). The calculated r_H changes from 1.14 for sample $x=0$ to 1.04 for sample $x=0.02$.

Pisarenko plot of S versus n_H can be calculated from Eqs. (1) and (2) and is presented in Fig. 3, together with the experimental data. The SPB model is reasonable in a region where minority carrier transport is negligible. This is typically the case in heavily doped (degenerate) semiconductors before thermal excitation of electron-holes pairs influences transport at high temperatures.[41] The measured Hall carrier concentration dependence of the Seebeck coefficient of the Co doped $Fe_{1-x}Co_xV_{0.6}Nb_{0.4}Sb$ samples matches the calculated lines well at 300, 400, and 500 K. The good agreement between experimental points and the calculated curves indicates that the effective mass m^* is almost independent of carrier concentration and temperature in the degenerate Co doped samples, and the single parabolic band model is applicable for analyzing the electrical transport in $Fe_{1-x}Co_xV_{0.6}Nb_{0.4}Sb$ compounds. The temperature dependence of Seebeck coefficient S was also calculated by the SPB model with the $m^*\approx2.0\,m_e$, given in Fig. 2(c). The results agree well with the experimental data before the intrinsic excitation. At higher temperatures, the experimental data have a large deviation from the calculated curves, due to the generation of electron-hole pairs from the thermal excitation, where the SPB model fails.

For a semiconductor with the single parabolic band and the acoustic phonon scattering, the Hall mobility can be expressed as

$$\mu_H=\mu_0\frac{F_{-1/2}(\eta)}{2F_0(\eta)}. \tag{5}$$

The value of μ_0 is related to the relaxation time τ_0 via $\mu_0=e\tau_0/m_I^*$, where m_I^* is the inertial effective mass. When the acoustic phonon scattering dominates the transport of charge carriers, μ_0 can be expressed as[42]

$$\mu_0=\frac{e\pi\hbar^4}{\sqrt{2}(k_BT)^{3/2}}\frac{v_l^2d}{E_{def}^2(m_b^*)^{5/2}}, \tag{6}$$

where v_l is the velocity of longitudinal sound waves, d is the density, and E_{def} is the deformation potential that represents the degree to which the charge carriers interact with phonons in a material.[27] m_b^* is expressed as $m^*=N_V^{2/3}m_b^*$, where N_v is

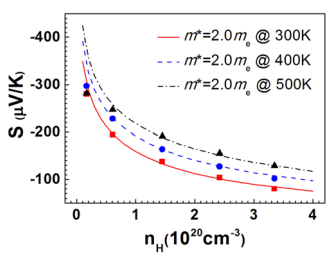

FIG. 3. Pisarenko plots of $Fe_{1-x}Co_xV_{0.6}Nb_{0.4}Sb$ ($x=0$, 0.005, 0.01, 0.015, 0.02) samples at 300, 400, and 500 K, respectively. The calculated curves (line) are generated assuming the $m^*=2.0m_e$ (m_e is the electron mass) under SPB model.

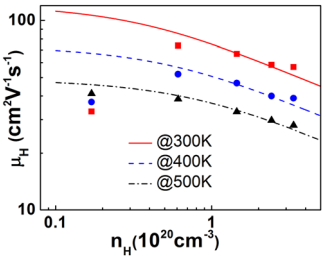

FIG. 4. Hall mobility versus Hall carrier concentration for $Fe_{1-x}Co_xV_{0.6}Nb_{0.4}Sb$ ($x = 0$, 0.005, 0.01, 0.015, 0.02) samples at 300, 400, and 500 K, respectively. The experimental data are compared to calculated SPB curves assuming carrier mobility is limited by acoustic phonon scattering.

the number of degenerate carriers pockets. The conduction band extrema of n-type FeVSb locates at X point of the Brillouin zone and has three equivalent pockets ($N_v = 3$), which dominate the transport properties.[12,37] The value v_l of ~5970 m/s was calculated from our previous measurement of low temperature specific heat.[36] Based on the acoustic phonon scattering using Eq. (6), the deformation potential E_{def} was calculated to be 14.1 eV by fitting the experimental carrier concentration dependence of mobility (in Fig. 4), which is in the reasonable range of 8 ~ 35 eV for a doped semiconductor.[43] A low deformation potential is beneficial for a relatively high carrier mobility.

Good TE materials in principle need a large $\mu m^{*3/2}$. For example, PbTe[44] has a small m^* but a large μ of several hundred $cm^2/V/s$ at room temperature. $Ba_8Ga_{16}Ge_{30}$[41] and La_3Te_4[45] have relative low μ (~10 $cm^2\ V^{-1}\ s^{-1}$) but large m^* ($1.8m_e$ for $Ba_8Ga_{16}Ge_{30}$ and $2.8m_e$ for La_3Te_4) at room temperature. In $Fe_{1-x}Co_xV_{0.6}Nb_{0.4}Sb$ half-Heusler compounds, the relatively large μ (40–80 $cm^2\ V^{-1}\ s^{-1}$ at room temperature), together with the relatively large m^* ($\sim 2.0m_e$) leads to a large $\mu m^{*3/2}$, which may explain why this system has high power factors.

Note that at low n_H ($1.5 \times 10^{20}\ cm^{-3}$), the experimental data deviate from the calculated curves in Fig. 4. For sample $x = 0$, the carrier concentration nearly keeps a constant (Fig. 2(b)), but the mobility μ_H increases with increasing temperature below 300 K (not shown here), not following the relationship $\mu_H \sim T^{-1.0}$, which indicates that additional scattering mechanism may exist in $FeV_{0.6}Nb_{0.4}Sb$. Heng *et al.*[46] recently reported that in PbS system the μ_H increases with increasing n_H at low carrier concentrations due to the polar optical phonon scattering and decreases with increasing n_H at higher carrier concentrations owing to the dominant acoustic phonon scattering.

IV. THERMAL CONDUCTIVITY

Fig. 5(a) shows the thermal conductivity κ increases with increasing Co content and decreases with temperature. At high temperatures, thermal conductivity increases due to the bipolar conduction. The measured specific heat, as shown in Fig. 5(a), increases with increasing temperature and the room temperature specific heat is approximately equal to the Dulong-Petit value (~0.306 J/g/K). The thermal conductivity is typically described as a sum of electronic and lattice contributions: $\kappa = \kappa_e + \kappa_L$. The Weidemann-Franz law permits

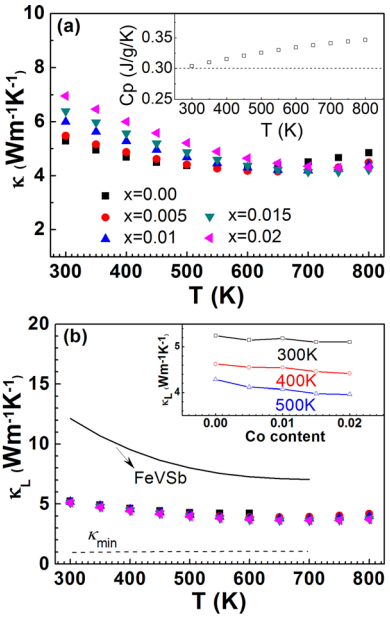

FIG. 5. Temperature dependences of thermal conductivity (a) and lattice thermal conductivity (b) of the $Fe_{1-x}Co_xV_{0.6}Nb_{0.4}Sb$ compounds. Inset of (a) shows the measured specific heat, and the dashed line represents the Dulong-Petit estimation. The inset in (b) shows the Co content dependence of lattice thermal conductivity at 300, 400, and 500 K, respectively. The solid line shows the ZT value of FeVSb from Ref. 35. κ_{min} was calculated according to Cahill's model.[47]

an estimation of the electronic component: $\kappa_e = L\sigma T$. L is Lorenz number and can be calculated by the single parabolic band approximation[41]

$$L = \frac{k_B^2}{e^2}\frac{3F_0(\eta)F_2(\eta) - 4F_1(\eta)^2}{F_0(\eta)^2}. \quad (7)$$

The calculated Lorenz constant for $Fe_{1-x}Co_xV_{0.6}Nb_{0.4}Sb$ compounds is in the range of $1.6 \times 10^{-8}\ V^2\ K^{-2} \sim 2.0 \times 10^{-8}\ V^2\ K^{-2}$, lower than the metallic limit L_0 of $2.45 \times 10^{-8}\ V^2\ K^{-2}$. The electron thermal conductivity κ_e for all the samples increases with increasing Co content and ranges from 0.1 W m^{-1} K^{-1} to 2.0 W m^{-1} K^{-1} at room temperature. At high temperatures, κ_e of the Co doped samples rapidly decreases and only contributes ~10% to the total thermal conductivity. Fig. 5(b) shows that the κ_L of $Fe_{1-x}Co_xV_{0.6}Nb_{0.4}Sb$ compounds is largely reduced compared with FeVSb. The Co content dependence of κ_L decreases slightly with increasing Co content, as shown in the inset of Fig. 5(b), which should be due to the enhanced alloy scattering induced by the difference in mass and atom radius between Fe and Co. The minimum thermal conductivity κ_{min} was calculated by Cahill's model.[47] The κ_L of all the $Fe_{1-x}Co_xV_{0.6}Nb_{0.4}Sb$ compounds is much higher than the minimum thermal conductivity κ_{min} (~1.0 W m^{-1} K^{-1}), suggesting that κ_L has still a large space to be reduced.

V. EFFECT OF BOUNDARY ON ELECTRON AND PHONON TRANSPORT

The free path length for the phonons varies strongly with their vibration frequency.[49] There are usually two approaches to reduce the lattice thermal conductivity in

half-Heusler compounds: one is to enhance the scattering of high frequency phonons by introducing point defects,[17,36] and the other is to enhance the scattering of low frequency phonons by grain refinement.[32,34] The point defect scattering has been introduced in FeVSb system by substituting Nb on the V sublattice and the lattice thermal conductivity was largely decreased.[36] Suppressing the propagation of low frequency phonons may be another effective way to further reduce the lattice thermal conductivity.

In order to benefit from the boundary scattering in thermoelectric materials, the PMFP should be smaller than the EMFP.[48] The estimation of PMFP and EMFP can give rough information on whether the grain refinement is effective in improving TE performance. When the acoustic phonon scattering of carriers is predominant in a large crystal, the mobility can be given by[49,50]

$$\mu = \frac{4el_e}{3(2\pi m_I^* k_B T)^{1/2}}, \tag{8}$$

where l_e is the electron mean free path. The phonon mean free path l_{ph} can be estimated from the lattice thermal conductivity using the equation

$$\kappa_L = \frac{1}{3} C_v v_s l_{ph}, \tag{9}$$

where C_v is the specific heat per unit volume, and v_s the sound velocity. The lattice thermal conductivity κ_L of sample $x = 0.1$ and $x = 0.015$ from 5–600 K is shown in Fig. 6(a). The slight increase in κ_L for sample $x = 0.01$ between ~200 K and 300 K is due to the radiation loss. The PMFP and EMFP of samples $x = 0.01$ and $x = 0.015$ were roughly estimated and shown in Fig. 6(b). The PMFP decreases with increasing temperature in the investigated temperature range. And the EMFP increases with increasing temperature and is ~5 nm above 100 K. At low temperatures, the PMFP is much larger than the EMFP, suggesting that boundary scattering may be effective in reducing lattice thermal conductivity while less affecting carrier mobility and electrical conductivity. However, above ~100 K, the EMFP is larger than PMFP, implying that grain refinement may reduce the carrier mobility more than the lattice thermal conductivity.

In order to validate the above analysis, two fine-grained samples $Fe_{0.99}Co_{0.01}V_{0.6}Nb_{0.4}Sb$ ($x = 0.01$BM) and $Fe_{0.985}Co_{0.015}V_{0.6}Nb_{0.4}Sb$ ($x = 0.015$BM) were prepared by BM followed by SPS. The typical SEM images of the samples $x = 0.01$ and $x = 0.01$BM are shown in Fig. 7. Sample $x = 0.01$, without ball milling, has larger particles of ~2.5 μm, while the ball milled sample $x = 0.01$BM possesses relatively smaller particles ranging from ~300 nm to 1 μm.

As shown in Fig. 8(a), the lattice thermal conductivity κ_L of the BMed samples has a distinct decrease compared to the coarse-grained counterparts. Especially at room temperature, a decrease of ~30% was obtained for the two BMed samples. Above the room temperature, the boundary scattering of phonons weakens with increasing temperature due to the reduced low frequency phonons. As a result, the decrease in high temperature κ_L is not as obvious as room temperature κ_L. However, the Hall mobility of the BMed samples also distinctly decreases. The ratio μ_H/κ_L of the BMed samples, as shown in Fig. 8(b), is reduced compared with that of the

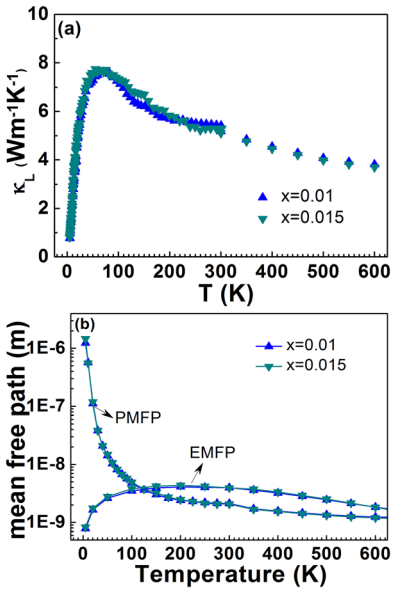

FIG. 6. Temperature dependences of lattice thermal conductivity (a) and EMFP and PMFP (b) for samples $x = 0.01$ and $x = 0.015$.

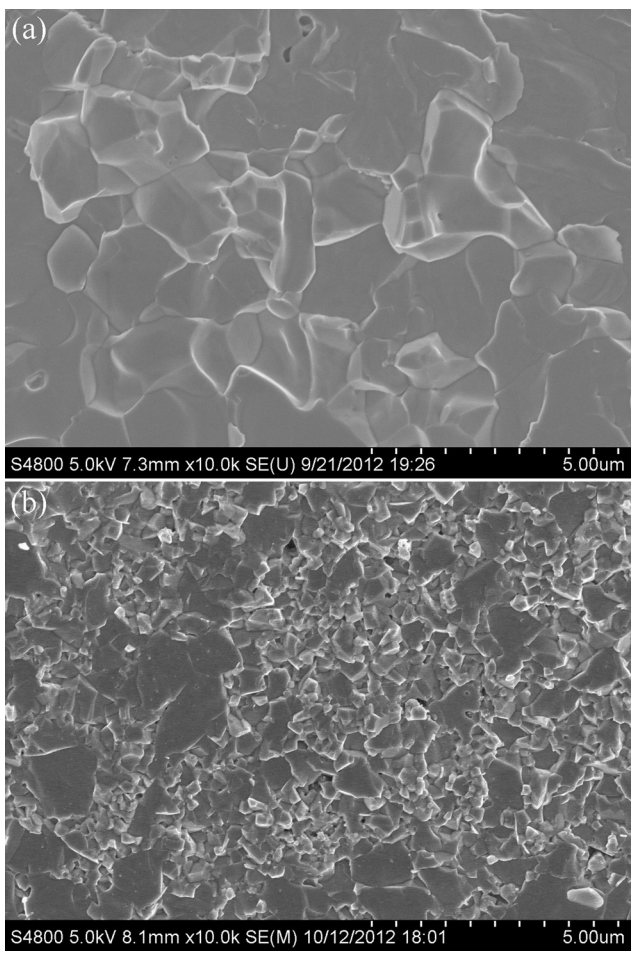

FIG. 7. SEM images of the fractured surface of samples $x = 0.01$(a) and $x = 0.01$BM (b).

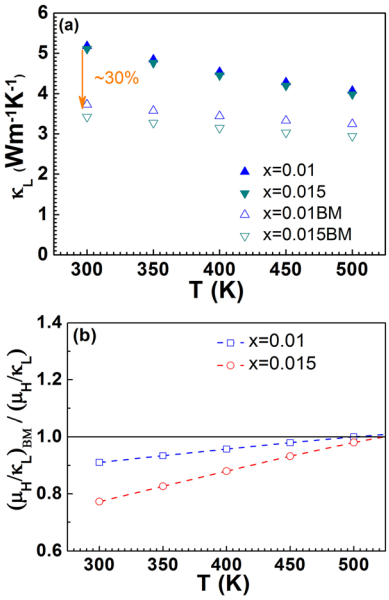

FIG. 8. Temperature dependence of lattice thermal conductivity κ_L (a) and the $(\mu_H/\kappa_L)_{BM}$ to (μ_H/κ_L) ratio (b) of the BMed and non-BMed samples.

coarse-grained counterparts, consistent with the above analysis on mean free path. Therefore, grain refinement will not contribute to the further improvement of TE performance for $Fe_{1-x}Co_xV_{0.6}Nb_{0.4}Sb$ compounds.

The temperature dependence of *ZT* value of the $Fe_{1-x}Co_xV_{0.6}Nb_{0.4}Sb$ compounds is shown in Fig. 9(a). The maximum *ZT* values of all the Co-doped samples are higher than that of FeVSb. A maximum *ZT* value of ~0.33 was obtained at 650 K for sample $x = 0.015$, an increase by ~60% compared with FeVSb. The *ZT* of the BMed samples $x = 0.01$BM and $x = 0.015$BM decreases, compared with the non-BMed counterparts, mainly due to the largely reduced mobility. The carrier concentration dependence of the *ZT* calculated by SPB model is shown in Fig. 9(b), together with the experimental data. The optimal Hall carrier concentration $n_{H,opt}$, at which the maximum *ZT* value occurs, is estimated to be $\sim 3.0 \times 10^{20}$ cm^{-3} at 600 K.

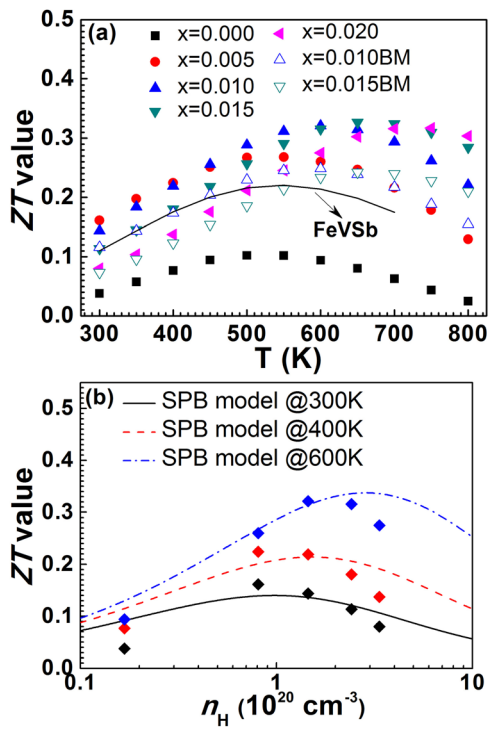

FIG. 9. (a) Temperature dependence of *ZT* value of the $Fe_{1-x}Co_xV_{0.6}Nb_{0.4}Sb$ compounds, the solid line shows the *ZT* of FeVSb from Ref. 35; (b) *ZT* value versus Hall carrier concentration for $Fe_{1-x}Co_xV_{0.6}Nb_{0.4}Sb$ samples from this study at different temperatures, and the lines were generated by SPB model.

VI. CONCLUSIONS

The electron and phonon transport of n-type $Fe_{1-x}Co_xV_{0.6}Nb_{0.4}Sb$ ($x = 0$-0.02) half-Heusler thermoelectric compounds was analyzed. The state density effective mass was determined to be ~$2.0m_e$. The deformation potential $E_{def} = 14.1$ eV was derived by a SPB model. And the band gap E_g is ~0.3 eV. The EMFP is several times larger than the PMFP above room temperature, suggesting that grain refinement is not an effective way in improving *ZT* of this system because the ratio of mobility to lattice thermal conductivity will decrease by enhancing boundary scattering. The subsequent experimental results corroborate the supposition. A maximum *ZT* value of ~0.33 was obtained at 650 K for sample $x = 0.015$ due to the carrier concentration optimization, ~60% increase compared with FeVSb. The optimal doping level was estimated to be $\sim 3.0 \times 10^{20}$ cm^{-3} at 600 K.

ACKNOWLEDGMENTS

This work was supported by the National Basic Research Program of China (2013CB632503), the Nature Science Foundation of China (Grant Nos. 51171171, 51271165, and 51101139), and the Program for New Century Excellent Talents in University (NCET-12-0495).

[1]T. Graf, C. Felser, and S. S. P. Parkin, Prog. Solid State Chem. **39**, 1 (2011).
[2]B. Balke, G. H. Fecher, A. Gloskovskii, J. Barth, K. Kroth, C. Felser, R. Robert, and A. Weidenkaff, Phys. Rev. B **77**, 045209 (2008).
[3]Z. Y. Zhu, Y. C. Cheng, and U. Schwingenschlögl, Phys. Rev. B **84**, 113201 (2011).
[4]S. Ouardi, G. H. Fecher, B. Balke, X. Kozina, G. Stryganyuk, C. Felser, S. Lowitzer, D. Ködderitzsch, and H. Ebert, Phys. Rev. B **82**, 085108 (2010).
[5]T. J. Zhu, L. Lu, M. O. Lai, and J. Ding, Smart Mater. Struct. **14**, S293 (2005).
[6]A. Roy, J. W. Bennett, K. M. Rabe, and D. Vanderbilt, Phys. Rev. Lett. **109**, 037602 (2012).
[7]H. Lin, L. A. Wray, Y. Q. Xia, S. Y. Xu, S. A. Jia, R. J. Cava, A. Bansil, and M. Z. Hasan, Nat. Mater. **9**, 546 (2010).
[8]S. Ouardi, C. Shekhar, G. H. Fecher, X. Kozina, G. Stryganyuk, C. Felser, S. Ueda, and K. Kobayashi, Appl. Phys. Lett. **98**, 211901 (2011).
[9]C. Uher, J. Yang, S. Hu, D. T. Morelli, and G. P. Meisner, Phys. Rev. B **59**, 8615 (1999).
[10]F. G. Aliev, V. V. Kozyrkov, V. V. Moshchalkov, R. V. Scolozdra, and K. Durczewshi, Z. Phys. B: Condens. Matter **80**, 353 (1990).
[11]J. Yang, H. Li, T. Wu, W. Zhang, L. Chen, and J. Yang, Adv. Funct. Mater. **18**, 2880 (2008).
[12]L. Jodin, J. Tobola, P. Pecheur, H. Scherrer, and S. Kaprzyk, Phys. Rev. B **70**, 184207 (2004).
[13]M. J. Kirkham, A. M. dos Santos, C. J. Rawn, E. Lara-Curzio, J. W. Sharp, and A. J. Thompson, Phys. Rev. B **85**, 144120 (2012).
[14]D. M. Rowe, *CRC Handbook of Thermoelectrics* (CRC Press, Boca Raton, FL, 2006).
[15]G. J. Snyder and E. S. Toberer, Nat. Mater. **7**, 105 (2008).

[16]S. Sakurada and N. Shutoh, Appl. Phys. Lett. **86**, 082105 (2005).
[17]J. Yang, G. P. Meisner, and L. Chen, Appl. Phys. Lett. **85**, 1140 (2004).
[18]M. S. Dresselhaus, G. Chen, M. Y. Tang, R. G. Yang, H. Lee, D. Z. Wang, Z. F. Ren, J. P. Fleurial, and P. Gogna, Adv. Mater. **19**, 1043 (2007).
[19]C. J. Vineis, A. Shakouri, A. Majumdar, and M. G. Kanatzidis, Adv. Mater. **22**, 3970 (2010).
[20]A. J. Minnich, M. S. Dresselhaus, Z. F. Ren, and G. Chen, Energy Environ. Sci. **2**, 466 (2009).
[21]J. P. Heremans, V. Jovovic, E. S. Toberer, A. Saramat, K. Kurosaki, A. Charoenphakdee, S. Yamanaka, and G. J. Snyder, Science **321**, 554 (2008).
[22]J. P. Heremans, B. Wiendlocha, and A. M. Chamoire, Energy Environ. Sci. **5**, 5510 (2012).
[23]W. Liu, X. Tan, K. Yin, H. Liu, X. Tang, J. Shi, Q. Zhang, and C. Uher, Phys. Rev. Lett. **108**, 166601 (2012).
[24]Y. Z. Pei, X. Y. Shi, A. LaLonde, H. Wang, L. D. Chen, and G. J. Snyder, Nature **473**, 66 (2011).
[25]Y. Z. Pei, A. D. LaLonde, N. A. Heinz, X. Y. Shi, S. Iwanaga, H. Wang, L. D. Chen, and G. J. Snyder, Adv. Mater. **23**, 5674 (2011).
[26]Y. Z. Pei, H. Wang, and G. J. Snyder, Adv. Mater. **24**, 6125 (2012).
[27]H. Wang, Y. Z. Pei, A. D. LaLonde, and G. J. Snyder, Proc. Natl. Acad. Sci. U.S.A. **109**, 9705 (2012).
[28]H. H. Xie, J. L. Mi, L. P. Hu, N. Lock, M. Chirstensen, C. G. Fu, B. B. Iversen, X. B. Zhao, and T. J. Zhu, Cryst. Eng. Commun. **14**, 4467 (2012).
[29]T. J. Zhu, K. Xiao, C. Yu, J. J. Shen, S. H. Yang, A. J. Zhou, X. B. Zhao, and J. He, J. Appl. Phys. **108**, 044903 (2010).
[30]H. H. Xie, C. Yu, T. J. Zhu, C. G. Fu, G. J. Snyder, and X. B. Zhao, Appl. Phys. Lett. **100**, 254104 (2012).
[31]W. J. Xie, J. He, S. Zhu, X. L. Su, S. Y. Wang, T. Holgate, J. W. Craff, V. Ponnambalam, S. J. Poon, X. F. Tang, Q. J. Zhang, and T. M. Tritt, Acta Mater. **58**, 4705 (2010).
[32]X. A. Yan, G. Joshi, W. S. Liu, Y. C. Lan, H. Wang, S. Lee, J. W. Simonson, S. J. Poon, T. M. Tritt, G. Chen, and Z. F. Ren, Nano Lett. **11**, 556 (2011).
[33]C. Yu, T. J. Zhu, R. Z. Shi, Y. Zhang, X. B. Zhao, and J. He, Acta Mater. **57**, 2757 (2009).
[34]X. Yan, W. S. Liu, H. Wang, S. Chen, J. Shiomi, K. Esfarjani, H. Z. Wang, D. Z. Wang, G. Chen, and Z. F. Ren, Energy Environ. Sci. **5**, 7543 (2012).
[35]C. G. Fu, H. H. Xie, Y. T. Liu, T. J. Zhu, J. Xie, and X. B. Zhao, Intermetallics **32**, 39 (2013).
[36]C. G. Fu, H. H. Xie, T. J. Zhu, J. Xie, and X. B. Zhao, J. Appl. Phys. **112**, 124915 (2012).
[37]D. P. Young, P. Khalifah, R. J. Cava, and A. P. Ramirez, J. Appl. Phys. **87**, 317 (2000).
[38]H. J. Goldsmid, *Electronic Refrigeration* (Pion Limited, London, 1986).
[39]X. Y. Shi, Y. Z. Pei, G. J. Snyder, and L. D. Chen, Energy Environ. Sci. **4**, 4086 (2011).
[40]H. J. Goldsmid and J. W. Sharp, J. Electron. Mater. **28**, 869 (1999).
[41]A. F. May, E. S. Toberer, A. Saramat, and G. J. Snyder, Phys. Rev. B **80**, 125205 (2009).
[42]H. J. Goldsmid, *Thermoelectric Refrigeration* (Plenum Press, New York, 2010).
[43]H. Wang, A. D. Lalonde, Y. Z. Pei, and G. J. Snyder, Adv. Funct. Mater. **23**, 1586 (2012).
[44]Y. Z. Pei, A. D. LaLonde, H. Wang, and G. J. Snyder, Energy Environ. Sci. **5**, 7963 (2012).
[45]A. F. May, E. Flage-Larsen, and G. J. Snyder, Phys. Rev. B **81**, 125205 (2010).
[46]H. Wang, E. Schechtel, Y. Z. Zhong, and G. J. Snyder, Adv. Energy Mater. **3**, 488 (2012).
[47]D. G. Cahill, S. K. Watson, and R. O. Pohl, Phys. Rev. B **46**, 6131 (1992).
[48]N. Satyala and D. Vashaee, Appl. Phys. Lett. **100**, 073107 (2012).
[49]H. J. Goldsmid, *Introduction to Thermoelectricity* (Springer, New York, 2010).
[50]J. W. Sharp, S. J. Poon, and H. J. Goldsmid, Phys. Status Solidi A **187**, 507 (2001).